Electrochimica Acta 306 (2019) 446–453

Contents lists available at ScienceDirect

Electrochimica Acta

journal homepage: www.elsevier.com/locate/electacta

Loofah-derived carbon as an anode material for potassium ion and lithium ion batteries

Zhenrui Wu [a], Liping Wang [a, *], Jie Huang [b], Jian Zou [a], Shulin Chen [c], Hua Cheng [d], Cheng Jiang [a], Peng Gao [c], Xiaobin Niu [a, **]

[a] School of Materials and Energy, State Key Laboratory of Electronic Thin Film and Integrated Devices, University of Electronic Science and Technology of China, Chengdu 610054, China
[b] Beijing WeLion New Energy Technology Co., LTD, Beijing 102402, China
[c] Electron Microscopy Laboratory, School of Physics, Peking University, Beijing 100871, China
[d] Department of Materials Science and Engineering, Southern University of Science and Technology, Shenzhen 518055, China

ARTICLE INFO

Article history:
Received 6 February 2019
Received in revised form
22 March 2019
Accepted 23 March 2019
Available online 23 March 2019

Keywords:
Biomass-derived carbon
Loofah
Potassium ion battery
Lithium ion battery
Chemical diffusion coefficient

ABSTRACT

In this work, we report a facile and inexpensive strategy to synthesize loofah-derived pseudo-graphite (LPG) through alkali treatment process followed by a one-step pyrolysis procedure. This mesoporous hard carbon material offers superb dual functionality for both lithium-ion battery (LIB) and potassium-ion battery (KIB) anodes. Tested against lithium and potassium, LPG delivers a specific capacity of 225 mAh·g^{-1} in LIBs and 150 mAh·g^{-1} in KIBs after 200 cycles at the current density of 100 mA g^{-1}. The good performance of LPG for both LIBs and KIBs mainly originates from its dual storage mechanism. On one hand, wider layered pseudo-graphite units provide space for Li^+/K^+ intercalation at higher voltages (>0.17 V in LIBs, > 0.56 V in KIBs). On the other hand, highly accessible mesoporous structure and defect-activated units in the near-surface region make it possible for Li^+/K^+ deposition at low voltages. The different performance of LPG in LIBs and KIBs may originate from varied ion-storage mechanisms. Despite the similar diffusion coefficient (D^+), lower capacity of LPG for potassium can be contributed to its limited intercalation kinetics in higher voltage (>0.56 V) and evidently higher resistance in the charge-transfer process (R_{ct}).

1. Introduction

These years, lithium ion batteries have become increasingly popular in the energy storage industry, which leads to significant consumption of lithium source. In addition, some transition metals (e.g. Co) used in lithium-ion batteries have limited resources [1]. As a result, to develop cheaper and more sustainable substitutes of LIBs can be important. Till now, various metal-ion batteries, such as sodium ion batteries (NIBs), potassium ion batteries (KIBs), aluminium ion batteries (AIBs) and dual ion batteries (DIBs) are studied [2–9]. Among these novel categories of batteries, NIBs attract much attention due to sodium's superb crust abundance and the 'rocking chair' electrochemical behaviour similar to that of LIBs [10].

However, potassium ion batteries represent a promising candidate as well for the following four advantages. First, potassium is an earth-abundant element compared to lithium, occupying 1.5 mass% vs. 0.0017 mass% of Li, and the cost of potassium is only about one-tenth of that of lithium [5]. Second, the electrode potential of potassium (−2.93 V vs. standard hydrogen electrode) is lower than that of sodium (−2.71 V vs. SHE) and close to that of lithium (−3.04 V vs. SHE.), allowing for a wider range of choices for possible cathode materials and higher voltage of batteries, assuring relatively more promising energy density of potassium-ion batteries. Third, aluminium as the anode current collector for KIBs is much lighter than copper, which may enable the gravimetric energy density of KIBs higher than that of LIBs. Fourth, despite the larger radius of K^+ may hinder the intercalation process, its good compatibility with some electrolytes such as 1,2-dimethoxyethane (DME) has been proved to achieve even smaller K^+-solvent Stroke's radius, which may show benefits for kinetics behaviours [11].

Till now, a variety of anode materials in potassium ion batteries

* Corresponding author.
** Corresponding author.
E-mail addresses: lipingwang@uestc.edu.cn (L. Wang), xbniu@uestc.edu.cn (X. Niu).

https://doi.org/10.1016/j.electacta.2019.03.165
0013-4686/

have been widely researched and developed, such as soft carbon [11–15], hard carbon (pyrolysis carbon, acetylene black), metal and metallic oxides (alloy) [16–21]. Among these materials, carbon shows superior benefits: abundant resources, decent potassium storage capacity, and mature fabrication process which has been widely used in commercialized LIBs industry. To be more exact, hard carbon, as many studies indicate, may achieve better rate performance owing to its natural 'pseudo-graphite' structure [20]. Moreover, compared to graphite as a type of soft carbon, hard carbon's dual storage mechanism in terms of inner-layer intercalation and near-surface absorption allows for faster kinetics process [22,23].

Here, we report a new type of hard carbon material, originated from loofah, widely planted in India, China, and Vietnam [24], achieving good electrochemical performance as anode materials in both LIBs and KIBs. Their electrochemical difference including capacity, chemical diffusion coefficient, charge transfer resistance, ion storage mechanisms are systematically explored. The advantage of the loofah derived carbon as biomass materials can be multifaceted: superb conductivity, sufficient activated units in the near-surface region, and special ion-storage structure. As a result, loofah derived carbon can be one of the most promising candidates of hard carbon anode materials for potassium storage.

2. Experimental

2.1. Materials and sample preparation

The loofah derived pseudo-graphite (LPG) was prepared by alkali treatment process followed by a one-step carbonization procedure. In details, first, commercial loofah was cut into $3 \times 3\ cm^2$ pieces and dried under vacuum at 60 °C for 24 h till the weight remained unchanged. Then dried loofah samples were treated by KOH (5 M) at 80 °C for 48 h and then ultrasonic-cleaned by D.I. water and ethanol separately three times (30 min each time) till the pH equalled to 7, after which the treated precursor was dried at 60 °C overnight in an oven before use. The dried sample was then pyrolysis in a tubular furnace at 1000 °C for 2 h under nitrogen atmosphere with a heating rate of $5\ °C \cdot min^{-1}$, and eventually became the loofah derived pseudo-graphite (LPG). High pyrolysis temperature and loofah's natural fibre-rich structure assured the highly conductive interconnected networks for electron transport. The alkali treatment removed impurities including SiO_2 and created abundant active surface sites for potassium storage.

2.2. Materials characterizations

Scanning Electron Microscopy (SEM) was tested by Hitachi S-4800 (Japan). Transmission electron microscopy (TEM) was performed using an aberration-corrected FEI Titan Themis G2 microscope operated at 80 kV. X-ray diffraction (XRD) patterns were recorded by X'Pert ProMPD using CuKα radiation (λ = 1.5418 Å) with a scan step of 0.02° in the 2θ range of 10°–70°. Raman measurements were performed using OTBP1218-200 with a 532 nm laser source (ZOLIX INSTRUMENTS CO., LTD.). TA instrument Q500 was used in the thermo-gravimetric analysis (TGA) under nitrogen atmosphere at a heating rate of $5\ °C \cdot min^{-1}$ from room temperature to 800 °C. Micromeritics ASAP202 was used to collect N_2 adsorption and desorption isotherms data at room temperature after pumping the samples. Barrentt-Joyner-Halenda (BJH) and Brunauer-Emmett-Teller (BET) methods were employed to estimate the mean pore diameter and specific surface area of LPG material respectively.

2.3. Cell assembling and electrochemical tests

The electrodes were prepared with a mixture of 80 wt% active materials, 10 wt% carbon black and 10 wt% PVDF binder in slurry from by addition of N-methyl-2-pyrrolidine (NMP) as solvent on copper foils, after which they were dried in vacuum oven at 110 °C for 10 h before assembling. The average loading of the active material per graphite electrode was about 1.0–2.0 mg cm^{-2}. Lithium or potassium was used as the counter electrode, glass fiber film were used as the separator. 1 M $LiPF_6$ or KPF_6 dissolved in ethylene carbonate (EC)/dimethyl carbonate (DMC) (1:1 by volume) was used as the corresponding electrolyte. 2032 coin cells were assembled in an argon-filled glove box. All the electrochemical tests were performed using a 2-electrode coin cell with LPG as a working electrode and lithium/potassium metal as a countering electrode.

Instrument CT2001A (LAND Electronic Co.) was applied in galvanostatic discharge-charge measurements with the range of 0.01–3.0 V. The cyclic voltammetry (CV) was tested using CHI660E electrochemical workstation (CH Instruments Ins). Electrochemical impedance spectroscopy (EIS) measurements were performed at the frequency range of 10 mHz ~ 0.1 MHz at an amplitude of 10 mV. Galvanostatic intermittent titration technique (GITT) measurements were performed by using a constant current density of 100 mA g^{-1} for 5 min then relaxing for 50 min.

3. Results and discussion

3.1. Morphology and structural characterizations

The LPG is prepared by a facile one-step process, and the schematic illustration of synthesis route is shown in Scheme 1. After the loofah fruit is mature, the outer skin is removed by drying, and the fiber-like inner part is loofah. The loofah is alkali-treated under 80 °C for 48 h, ultrasonically cleaned and dried, then carbonized under N_2 atmosphere at 1000 °C for 2 h. Due to the alkali removed some particles and the moderate lignin precipitated at 550 °C, loose mesoporous structure carbon materials are achieved. To verify whether the removal of SiO_2 by alkali treatment attribute to the form of mesoporous structure of LPG, further experiment is designed (Fig. S1). Untreated raw loofah is directly burned in air under 1000 °C for 2 h and left some white skeleton-like residue, which cannot be fully dissolved by 37% HCl solution. With addition to KOH treatment, most white residuals are removed, which may indicate the existence of SiO_2.

The general structure of LPG examined by scanning electron microscopy (SEM) and transmission electron microscopy (TEM) are shown in Fig. 1. The SEM images of unmeshed LPG skeleton reveal the fiber-rich nature of the biomass derived carbon materials. To be more exact, on the millimeter scale, loofah carbon is a three-dimensional porous carbon framework in which a large number of plant fibers overlap each other, as shown in Fig. 1a. On the micrometer scale, each fiber is formed by the adhesion of hundreds of microfilament units, each of which is a hollow tubular structure, as shown in Fig. 1b. The cross-sectional view in Fig. 1c also corroborates such honeycomb-like one-way microtubule structure. TEM characterizes the structure of microfibers on a more precise scale (Fig. 1d–f). Fig. 1e illustrates the morphology of a single microfilament unit, and Fig. 1f characterizes the ordered arrangement of carbon atoms on the surface of the inner-hollowed microfibers. In this way, LPG as a type of hard carbon has a "house of cards" structure containing graphite-like micro crystallites and amorphous structure, the micro crystallites consist of few approximately parallel graphene sheets stacked together with large d-spacing (3.448 Å) as shown in Fig. 1e. Besides, these materials may have numerous active sites on the surface such as edges,

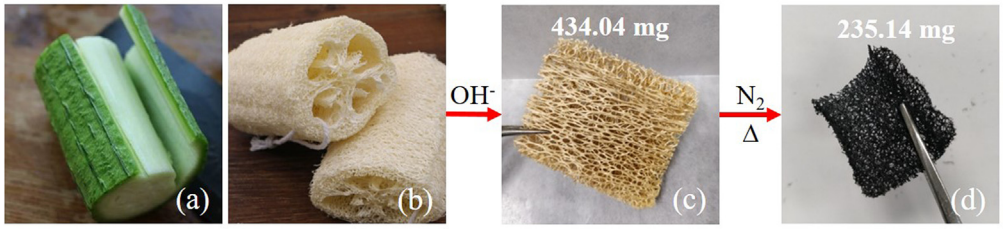

Scheme 1. Raw loofah (a) was dried and skin-peeled as dried loofah (b), then was treated by alkali at 60 °C for 48 h and then ultrasonic-cleaned by D.I. water and ethanol. Treated loofah (c) was carbonized in N_2 under 1000 °C for 2 h and became carbonized loofah (d).

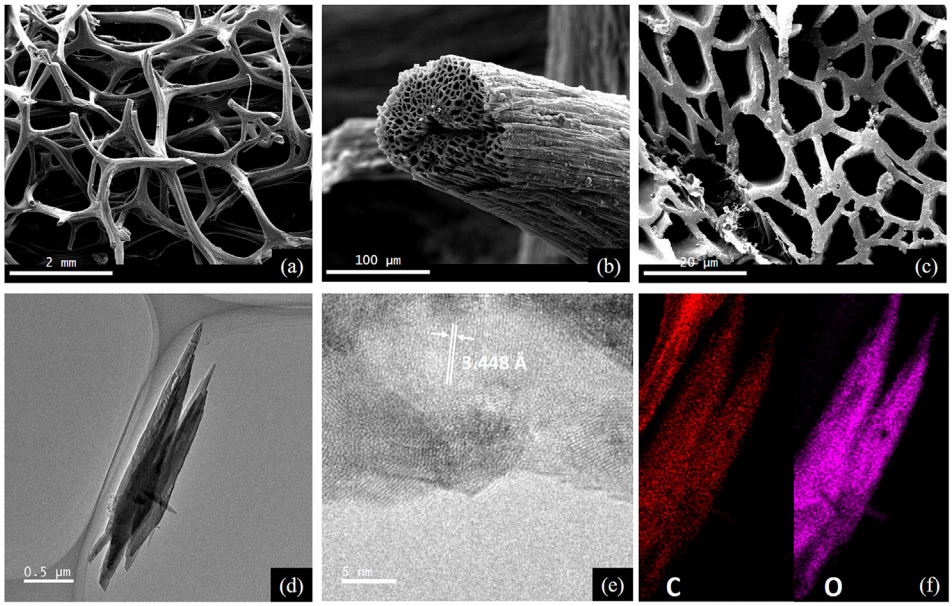

Fig. 1. SEM (a–c) and TEM (d–f) of loofah-derived pseudo-graphite (LPG).

defects and functional groups containing oxygen as electron-rich units as shown in Fig. 1f.

Thermo-gravimetric analysis (TGA) are performed to elaborate the very detailed categories of weight-lost in the fabrication of LPG anode materials. Studies indicate that biomass mainly consists of cellulose, hemicellulose, and lignin [25]. Among these three chemicals, hemicellulose is the most unstable component in pyrolysis, decomposing at ~225–325 °C; cellulose is in pyrolysis at a higher temperature of 325–375 °C; lignin gradually decomposes in a wide temperature range of ~500 °C [26]. In detail, hemicellulose and cellulose become volatile products after thermal decomposition, while lignin mainly forms charcoal and then turns into more orderly arranged carbon materials [27]. As shown in Fig. 2a, the pyrolysis of loofah can be divided into three stages: in the first stage, the weight shrinks moderately by ~7% under 200 °C, which could be attributed to the precipitation and internal recombination of free water in the biomass, releasing small molecules such as H_2O and CO_2; in the second stage (240–450 °C), the weight significantly decreases due to the cellulose and hemicellulose continuously decomposes into small molecules with high volatility, which are removed by the flowing N_2 in the tubular furnace; in the third stage (>500 °C), the weight loss becomes slight again, indicating that the pyrolysis of cellulose and hemicellulose has almost finished and lignin's slow decomposition just starts. Moreover, as the temperature increases, the internal volatiles slowly precipitate and gradually form a loose porous structure.

BET absorption test (Fig. 2b) indicates the materials possessing higher specific surface area (270 $m^2 g^{-1}$ vs. ~135 $m^2 g^{-1}$ for rice husk derived carbon) and larger mean pore diameter (3.6 nm vs. ~ 2.7 nm for coconut-derived activated carbon) [28–30]. Furthermore, the microstructure of the LPG is identified by X-ray diffraction (XRD). As shown in Fig. 2c, two main broad diffraction peaks at 25.7° and 43.2° are detected, corresponding to (002) and (101) diffractions of graphite (JCPDS No. 41–1487), respectively [31]. The peak imparted to the (101) diffraction is weak, indicating the relatively low graphitization degree of this carbon material. According to Bragg equation, an inter-plane d-spacing of 3.466 Å (slightly wider than 3.35 Å, the d-spacing of standardized graphite) can be calculated, and this result is similar to the d = 3.448 Å estimated in the TEM profiles.

Moreover, Raman spectra is employed to analyse the LPG's structure. Fig. 2d illustrates two summits located at 1335 and 1593 cm^{-1} which are related to the D-band and G-band, respectively. To be more exact, the intensity of D-band can evaluate the degree of sp^3 sufficiency in diamond-like carbon materials, representing heterogeneity and defects in the near-surface region of LPG units, while the G-band represents sp^3 vibration in graphite-like materials and reflects the homogeneity [32]. As a result, the ratio of D-band and G-band's intensity (I_D/I_G) in LPG is 1.106, much higher than standard graphite, which indicates the defective incoherence in a larger scale, and these defects provide enough absorption energy for the 'surface-drive' storage of potassium ions. In addition, some studies utilize the intensity ratio of 2D-band and G-band to shed light on the layer number of pseudo-graphite materials

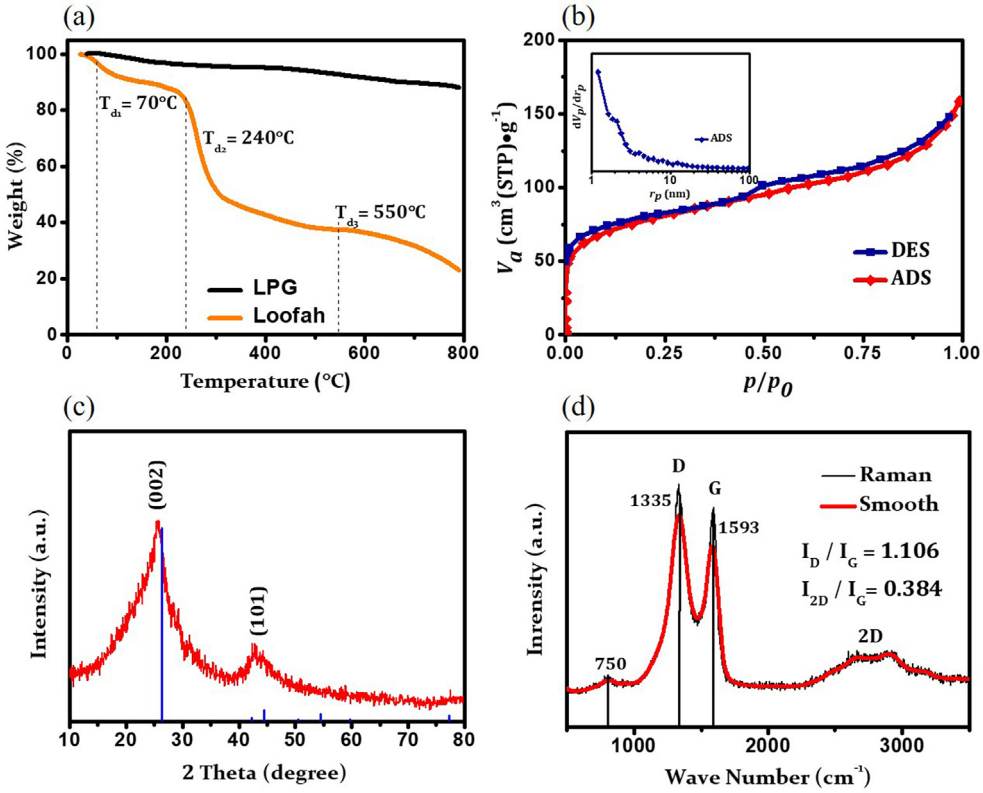

Fig. 2. TGA (a) analysis of loofah precursor. BET (b), XRD pattern (c), and Raman Spectra (d) of loofah-derived pseudo-graphite (LPG).

because in principle, I_{2D}/I_G equals to 2.3 for single layer graphene and this ratio would decrease to zero as the layer number growing. In this work, this ratio equals to 0.384, which represents thicker micro-crystal units. To be more exact, 2D wide peak can be manually divided into three pairs of subordinate Lorenz peaks (Fig. S2). In this way, the average number of layers in these pseudo-graphite units is at least three [33]. Such structure also assures a high surface area of 270 $m^2\,g^{-1}$ and a BJH pore volume of 0.167 $cm^3\,g^{-1}$.

3.2. Electrochemical measurements

To investigate the electrochemical performances of LPG, we carry out a series of electrochemical measurements using different categories of electrolytes in LIBs and KIBs. In LIBs, LPG as the anode achieves good cycling performance in three electrolytes: EC/DMC (Fig. 3a), EC/DEC and DOL/DME (Fig. S3), obtaining high specific capacity of 225 $mAh\cdot g^{-1}$ after 200 cycles at the current density of 100 $mA\,g^{-1}$ (~0.5C). As shown in Fig. 3b and Fig. S3, two distinct voltage regions have been observed, a steep slope above 1 V and a much more moderate one below 0.3 V, which may be contributed to dual kinetics process: Li^+ deposition in near-surface defective region and insertion into pseudo-graphite layers, respectively. In KIBs, this biomass derived carbon achieves 155 $mAh\cdot g^{-1}$ of reversible capacity in EC/DMC after 200 cycles without evident decay (Fig. 3c–d). However, as shown in Fig. S2, the electrochemical performance of LPG in DME assembled KIBs is evidently unstable, lasting for less than 50 cycles. Some studies tend to indicate the large capacity decay in this case originating from the incompatibility between KPF_6 and DME, while KFSI-DME has achieved stable reversible K^+ insertion/extraction [34–36].

To evaluate the rate performance of this material, charge/discharge tests at different current density from 20 $mA\,g^{-1}$ to 500 $mA\,g^{-1}$ are carried out. Fig. 4a displays the good rate performance of LPG in LIBs, which is capable of remaining its reversibly initial specific capacity at ~225 $mAh\cdot g^{-1}$ after 100 cycles even under a relatively higher current density, fulfilling the increasing demand for high-rate charge/discharge energy storage devices. Moreover, as shown in Fig. 4b, LPG in KIBs also remains at ~150 $mAh\cdot g^{-1}$ after 200 cycles in the same current density. LPG as both LIBs and KIBs anode demonstrates good electrochemical performances as compared with the reported biomass-derived carbon (Table S1 and S2).

Furthermore, cyclic voltammetry (CV) measurements are performed to investigate the different storage mechanism of Li^+ and K^+ in LPG in carbon-based and ether-based electrolyte (Fig. 4c–d and Fig. S4). It is notable that in EC/DMC an irreversible peak at 0.61 V versus Li^+/Li in the first cycle is detected and then disappears in the subsequent cycles, which may originate from the decomposition of the electrolyte and the formation of the solid electrolyte interphase (SEI) layer [37]. Moreover, a relatively wider redox peak was discovered in KIBs in a broad potential range of 0.01–0.6 V in contrast to the more acute peak in LIBs in 0.01–0.3 V, corresponding to the difficulties of potassium ions to intercalate into layered pseudo-graphite units of LPG electrode [32]. This result can be explained by the larger radius of K^+ (1.38 Å) compared with that of Li^+ (0.76 Å), and the larger radius would hinder its diffusion and intercalation. In EC/DMC, LPG has only a single oxidation peak in the charging process in both KIBs and LIBs referring to the de-intercalation of K^+ and Li^+ from LPG anodes, and the peak is located at 0.56 V for K^+ and 0.17 V for Li^+. In DME, the curves are evidently different: as shown in Fig. S4e, representing two pairs of redox peaks at 0.24 V/~0.01 V and 0.59 V/0.22 V, except for the redox peak at 1.01 V corresponding to the irreversible K^+ deposition and side-reactions of electrolytes.

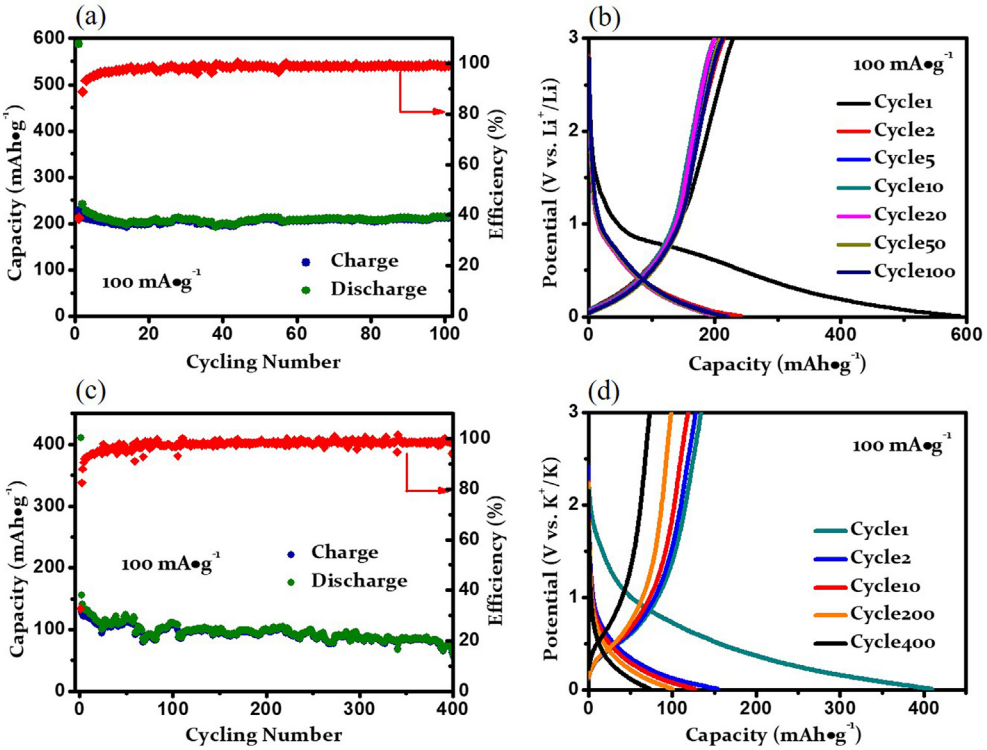

Fig. 3. Cycling (a, c), capacity (b, d) of loofah-derived pseudo-graphite (LPG) as lithium ion battery anode (a, b) and potassium ion battery anode (c, d) in EC/DMC-based electrolyte.

3.3. Kinetics and mechanisms

Galvanostatic intermittent titration technique (GITT) is introduced to test the thermodynamic operational voltage. As shown in Fig. 5a–b, the polarization potential ΔV in LIB profile is ~0.2 V on average, which is smaller than that in KIBs (~0.6 V). In addition, the equilibrium state curve (blue color) with a step-by-step plateau indicates a typical phase-to-phase transition mechanism of LiC_x in

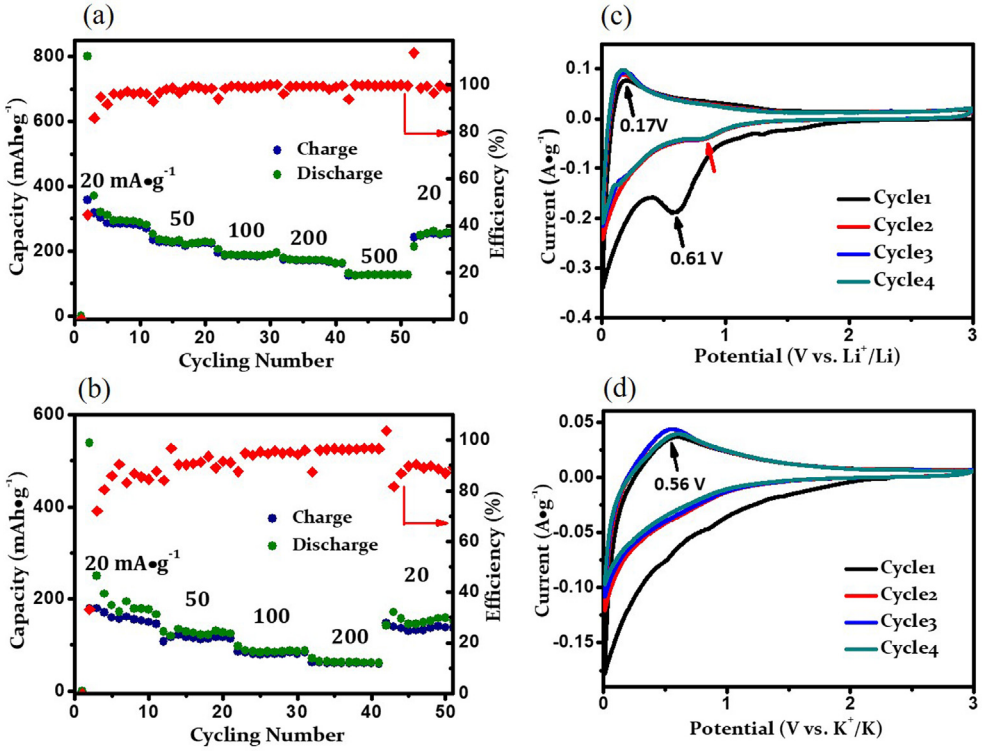

Fig. 4. Rate performance (a, b), and CV (c, d) of loofah-derived pseudo-graphite (LPG) as lithium ion battery anode (a, c) and potassium ion battery anode (b, d) in EC/DMC-based electrolyte.

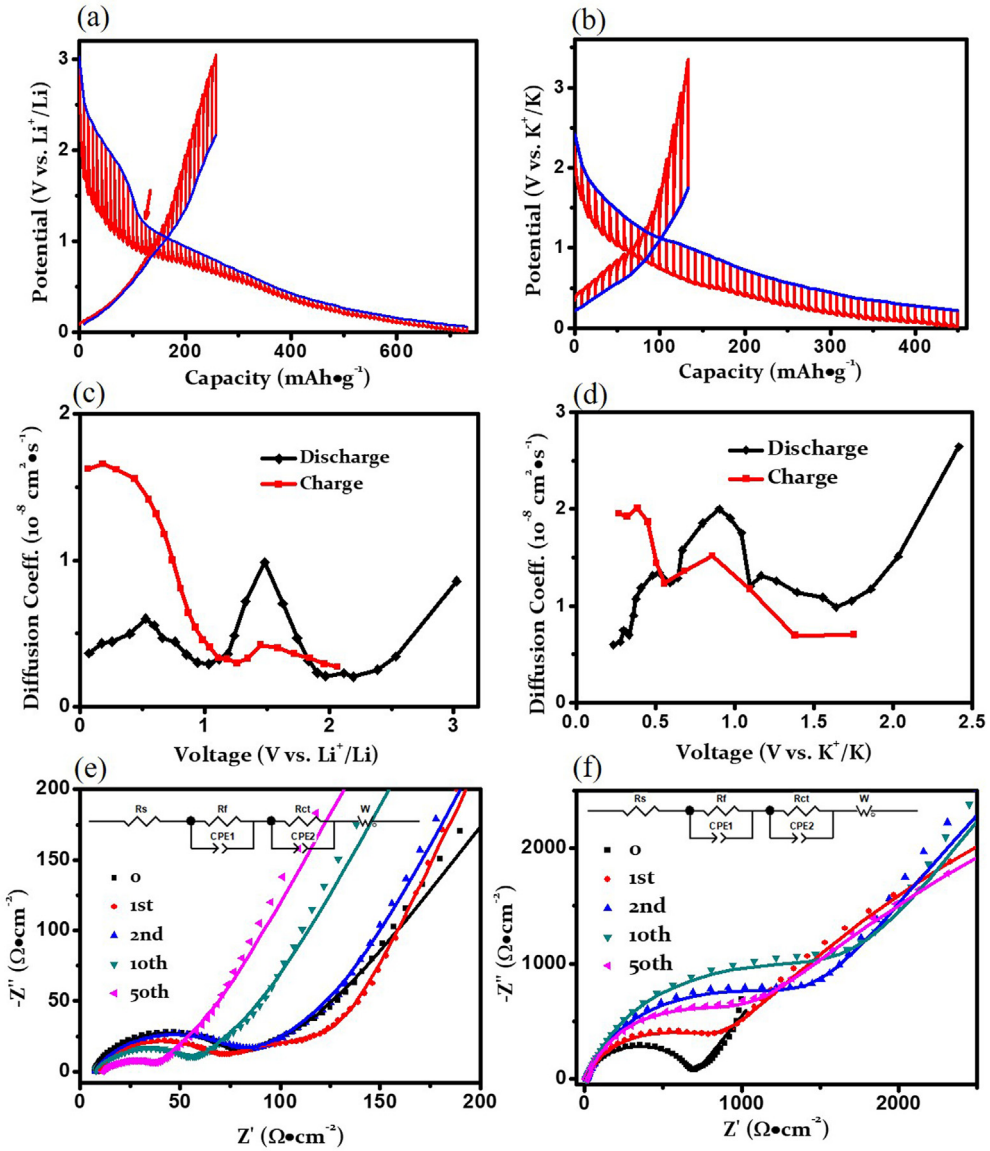

Fig. 5. The kinetics properties of loofah-derived pseudo-graphite (LPG) anode vs lithium (a, c, e) and potassium (b, d, f) are depicted by GITT (a–b), Diffusion coefficient (c–d), and electrochemical impedance spectra (e–f) with simulated equivalent circuits.

LIBs [38]. However, in terms of KIBs, the curve turns out to be a steady slope, which corroborate the 'surface-drive' storage mechanism. To be more exact, the voltage-capacity curve in the LIBs is much more complicated with both a phase-to-phase transition at ~1 V and a slight metallic deposition behaviour above 1 V. Moreover, a minimal charge/discharge voltage hysteresis is observed, which indicates LPG an analogue to graphite but on a more limited scale [39], which is in line with the previous analysis of Raman spectra.

We have also calculated the Li^+ and K^+ diffusion coefficient in EC/DMC system based on the GITT results using the equation [18].

$$D_{K^+} = \frac{4}{\pi}\left(\frac{m_B V_M}{M_B S}\right)^2 \left(\frac{\Delta E_S}{\tau(dE_\tau/d\sqrt{\tau})}\right)^2 \approx \frac{4}{\pi\tau}\left(\frac{m_B V_M}{M_B S}\right)^2 \left(\frac{\Delta E_S}{\Delta E_\tau}\right)^2 \left(\tau << L^2/D_{K^+}\right)$$

Where m_B is the mass (0.0017 g in KIBs and 0.0008 g in LIBs), M_B is the molecular weight of carbon (12.01 g mol^{-1}), V_M is the molar volume of hard carbon (42.74 cm^3 mol^{-1}), S is the effective area of the electrode (1.13 cm^2), $dE\tau/d\tau$ is the slope of the linearized proportional of the $E\tau$ during the deposition or decomposition process of duration time τ(s), $\triangle$Es is the potential change after every equilibrium process, L is the thickness of the electrodes [18]. We have obtained both diffusion coefficients of Li^+ and K^+ at ~10^{-8} cm^2 s^{-1} in EC/DMC system as shown in Fig. 5c and d, which hints that the kinetics capabilities of these bifurcated ion-storage mechanisms are quite similar.

Electrochemical impedance spectroscopy (EIS) at the charging state is employed to explore the kinetics difference in KIBs and LIBs (Fig. 5e and f). It is confirmative that the charge-transfer resistance R_{ct} in LIBs (<80 Ω) is much smaller than that in KIBs (>3000 Ω after first cycle), which hints that Li^+ is easier to intercalate into layered pseudo-graphite units. In addition, the Warburg resistance corresponding to ion diffusion in the electrolyte in LIBs is less significant than that in KIBs, indicating a lower-impedance ion transportation of Li^+. Moreover, the R_{ct} in KIBs significantly grows from 207 Ω to

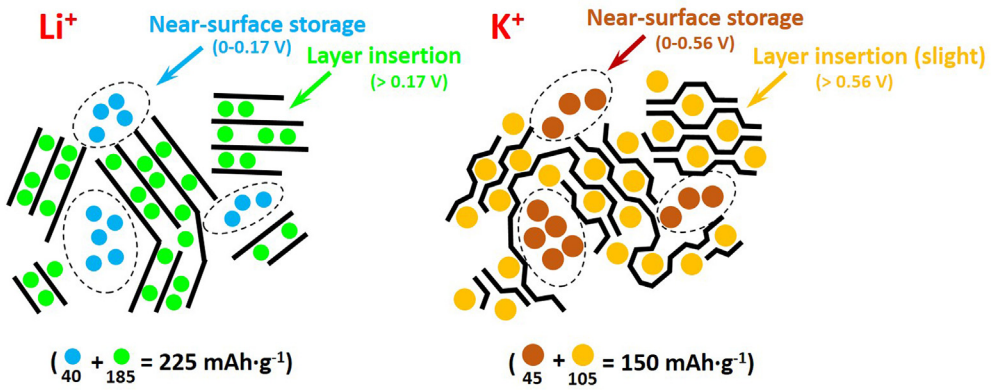

Fig. 6. Dual-ion storage mechanisms of Li^+ and K^+ in loofah-derived pseudo-graphite (LPG) materials.

over 3571 Ω after the first cycle, followed by a moderate growth to over 5000 Ω at the 50th cycle. This result may indicate a pre-potassiation procedure in KIBs in the initial cycles before the impedance returns to be stable, corroborating the aforementioned step-by-step dual mechanism in the previous CV analysis. Moreover, such a dramatic increase initially may relate to a high-speed loss of electrochemical active sites in this stage, which may result in the huge volume expansion and irreversible potassium accumulation [40]. According to CV of LIBs in Fig. 3d, the formation of SEI in LIBs is slight, which is also proved by its minimal $R_f < 80\ \Omega$ even after 100 cycles in contrast to that in KIBs at ~800 Ω (Fig. S5).

Studies on Li^+/K^+ storage mechanism in graphite/hard carbon have been carried out. Different from the intercalation mechanism of Li^+ involving ion-diffusion and insertion/extraction, K^+ storage in hard carbon can be more surface-driven [41]. Because of the large radius leading to kinetics impedance, potassium ions are difficult to intercalate into graphite layers under normal experimental conditions in principle. Instead, K^+ may deposit on the surface of micro graphite-like units known as 'surface-driven storage'. To be more exact, this process mainly happens on the defect-activated units in the near-surface region, wide space outside the micro-graphite particles enables favourable kinetics. Moreover, in hard carbon, carbon layers are randomly arranged, and this disordered arrangement facilitates intercalation of potassium ions: because of the larger radius of K^+ (1.38 Å) in contrast to Li^+ (0.76 Å) and Na^+ (1.02 Å) hindering its intercalation between layers, the structure of the anode materials can be well maintained due to the absence of alkali metal ion insertion/extraction. In this way, the longevity of batteries may be prolonged.

Although some studies have tried to figure out ion interactions with hard carbon, their specific storage mechanisms in voltage regions is still in veil. According to the electro-kinetics analysis, we report a dual mechanism as depicted in Fig. 6. To be more exact, during the initial discharge process (0–0.17 V for Li^+, 0–0.56 V for K^+), alkali metal ions are adsorbed in the near-surface region of hard carbon activated by heterogeneous atoms and various defects with a wide adsorption energy distribution, producing a sloping voltage profile. In the subsequent stage (0.17–3 V for Li^+, 0.56–3 V for K^+), ions intercalate into graphitic layers if suitable space is provided to form AC_x (A = alkali metal ions, LiC_6 and KC_8) compounds, producing a flat low voltage plateau [42,43]. However, considering the different radius of Li^+, Na^+, and K^+, potassium ions are considered more difficult to intercalate into layered graphite: as shown in Fig. 4d, the CV profile of KIBs is absent of the aforementioned flat plateau corresponding to the intercalation mechanism.

4. Conclusions

To summarize, this work reports an easily fabricated loofah derived pseudo-graphite (LPG) anode material with reversible specific capacity of 225 $mAh \cdot g^{-1}$ in Li-ion batteries and 150 $mAh \cdot g^{-1}$ in K-ion batteries, allowing for a promising prospect of further practical application in the battery industry as one of the effective and cheap alternatives of graphite. Moreover, LPG served as the anode material achieves decent rate performance (~130 $mAh \cdot g^{-1}$ at 500 mA g^{-1} in Li-ion batteries and ~70 $mAh \cdot g^{-1}$ at 200 mA g^{-1} in K-ion batteries) and excellent cycling stability (225 $mAh \cdot g^{-1}$ after 400 cycles at a current density of 100 mA g^{-1} with Coulombic efficiency nearly 100%). The good electrochemical performance of LPG can be contributed to the dual-ion storage mechanism due to the graphite-like units on the micron scale and the near-surface defects on a larger scope. Our work not only visualizes the possibility of biomass carbon application as an anode material for KIBs and LIBs, but sheds light on a novel strategy to manufacture cost-friendly and environment-friendly electrode materials for the energy storage industry.

Acknowledgements

This work is supported by the National Natural Science Foundation of China (51502032), the Fundamental Research Funds for the Central Universities, China (No. ZYGX2016J044) and the Opening Project of State Key Laboratory of Advanced Chemical Power Sources (SKL-ACPS-C-12). Hua Cheng acknowledges the support from the Basic Research Project of the Science and Technology Innovation Commission of Shenzhen (No. JCYJ20170817110251498), the Guangdong Special Support for the Science and Technology Leading Young Scientist (No. 2016TQ03C919), and the National Natural Science Foundation of China (No. 21603094).

Appendix A. Supplementary data

Supplementary data to this article can be found online at https://doi.org/10.1016/j.electacta.2019.03.165.

References

[1] H. Vikström, S. Davidsson, M. Höök, Lithium availability and future production outlooks, Appl. Energy 110 (2013) 252–266.
[2] W. Luo, F. Shen, C. Bommier, H. Zhu, X. Ji, L. Hu, Na-ion battery anodes: materials and electrochemistry, Acc. Chem. Res. 49 (2016) 231–240.
[3] M.D. Slater, D. Kim, E. Lee, C.S. Johnson, Sodium-ion batteries, Adv. Funct. Mater. 23 (2013) 947–958.

[4] M.-S. Balogun, Y. Luo, W. Qiu, P. Liu, Y. Tong, A review of carbon materials and their composites with alloy metals for sodium ion battery anodes, Carbon 98 (2016) 162–178.
[5] J.C. Pramudita, D. Sehrawat, D. Goonetilleke, N. Sharma, An initial review of the status of electrode materials for potassium-ion batteries, Adv. Energy Mater. 7 (2017), 1602911.
[6] M.-C. Lin, M. Gong, B. Lu, Y. Wu, D.-Y. Wang, M. Guan, M. Angell, C. Chen, J. Yang, B.-J. Hwang, An ultrafast rechargeable aluminium-ion battery, Nature 520 (2015) 324.
[7] B. Ji, F. Zhang, X. Song, Y. Tang, A novel potassium-ion-based dual-ion battery, Adv. Mater. 29 (2017), 1700519.
[8] Z. Jian, Y.S. Hu, X. Ji, W.J.A.M. Chen, Nasicon-structured Materials for Energy Storage, vol. 29, 2017, 1601925.
[9] Z. Jian, W. Luo, X. Ji, Carbon electrodes for K-ion batteries, J. Am. Chem. Soc. 137 (2015) 11566–11569.
[10] Q. Wang, B. Zhao, S. Zhang, X. Gao, C. Deng, Superior sodium intercalation of honeycomb-structured hierarchical porous $Na_3V_2(PO_4)_3$/C microballs prepared by a facile one-pot synthesis, J. Mater. Chem. 3 (2015) 7732–7740.
[11] Y.-H. Zhu, Q. Zhang, X. Yang, E.-Y. Zhao, T. Sun, X.-B. Zhang, S. Wang, X.-Q. Yu, J.-M. Yan, Q. Jiang, Reconstructed orthorhombic V_2O_5 polyhedra for fast ion diffusion in K-ion batteries, Chemistry 5 (2019) 168–179.
[12] W. Luo, J. Wan, B. Ozdemir, W. Bao, Y. Chen, J. Dai, H. Lin, Y. Xu, F. Gu, V. Barone, Potassium ion batteries with graphitic materials, Nano Lett. 15 (2015) 7671–7677.
[13] X. Wang, K. Han, D. Qin, Q. Li, C. Wang, C. Niu, L. Mai, Polycrystalline soft carbon semi-hollow microrods as anode for advanced K-ion full batteries, Nanoscale 9 (2017) 18216–18222.
[14] K. Share, A.P. Cohn, R.E. Carter, C.L. Pint, Mechanism of potassium ion intercalation staging in few layered graphene from in situ Raman spectroscopy, Nanoscale 8 (2016) 16435–16439.
[15] R.A. Adams, J.-M. Syu, Y. Zhao, C.-T. Lo, A. Varma, V.G. Pol, Binder-free N-and O-rich carbon nanofiber anodes for long cycle life K-ion batteries, ACS Appl. Mater. Interfaces 9 (2017) 17872–17881.
[16] C. Chen, Z. Wang, B. Zhang, L. Miao, J. Cai, L. Peng, Y. Huang, J. Jiang, Y. Huang, L. Zhang, J. Xie, Nitrogen-rich hard carbon as a highly durable anode for high-power potassium-ion batteries, Energy Storage Mater. 8 (2017) 161–168.
[17] M. Chen, W. Wang, X. Liang, S. Gong, J. Liu, Q. Wang, S. Guo, H. Yang, Sulfur/oxygen codoped porous hard carbon microspheres for high-performance potassium-ion batteries, Adv. Energy Mater. (2018), 1800171.
[18] Z. Jian, Z. Xing, C. Bommier, Z. Li, X. Ji, Hard carbon microspheres: potassium-ion anode versus sodium-ion anode, Adv. Energy Mater. 6 (2016), 1501874.
[19] F. Wu, L. Liu, Y. Yuan, Y. Li, Y. Bai, T. Li, J. Lu, C. Wu, Expanding interlayer spacing of hard carbon by natural K^+ doping to boost Na-ion storage, ACS Appl. Mater. Interfaces 10 (2018) 27030–27038.
[20] Z. Jian, S. Hwang, Z. Li, A.S. Hernandez, X. Wang, Z. Xing, D. Su, X. Ji, Hard-soft composite carbon as a long-cycling and high-rate anode for potassium-ion batteries, Adv. Funct. Mater. 27 (2017), 1700324.
[21] L. Wang, W. Jia, X. Liu, J. Li, M.M. Titirici, Sulphur-doped ordered mesoporous carbon with enhanced electrocatalytic activity for the oxygen reduction reaction, J. Energy Chem. 25 (2016) 566–570.
[22] Z. Jian, C. Bommier, L. Luo, Z. Li, W. Wang, C. Wang, P.A. Greaney, X. Ji, Insights on the mechanism of Na-ion storage in soft carbon anode, Chem. Mater. 29 (2017) 2314–2320.
[23] W. Chen, C. Chen, X. Xiong, P. Hu, Z. Hao, Y. Huang, Coordination of surface-induced reaction and intercalation: toward a high-performance carbon anode for sodium-ion batteries, Adv. Sci. 4 (2017), 1600500.
[24] W. Porterfield, Loofah—the sponge gourd, Econ. Bot. 9 (1955) 211–223.
[25] V. Pasangulapati, K.D. Ramachandriya, A. Kumar, M.R. Wilkins, C.L. Jones, R.L. Huhnke, Effects of cellulose, hemicellulose and lignin on thermochemical conversion characteristics of the selected biomass, Bioresour. Technol. 114 (2012) 663–669.
[26] R. Yuan, S. Yu, Y. Shen, Pyrolysis and combustion kinetics of lignocellulosic biomass pellets with calcium-rich wastes from agro-forestry residues, Waste Manag. 87 (2019) 86–96.
[27] H. Yang, R. Yan, H. Chen, D.H. Lee, C. Zheng, Characteristics of hemicellulose, cellulose and lignin pyrolysis, Fuel 86 (2007) 1781–1788.
[28] S. Guo, J. Peng, W. Li, K. Yang, L. Zhang, S. Zhang, H. Xia, Effects of CO_2 activation on porous structures of coconut shell-based activated carbons, Appl. Surf. Sci. 255 (2009) 8443–8449.
[29] M.A. Yahya, Z. Al-Qodah, C.Z. Ngah, Agricultural bio-waste materials as potential sustainable precursors used for activated carbon production: a review, Renew. Sustain. Energy Rev. 46 (2015) 218–235.
[30] L. Wang, Z. Schnepp, M.M. Titirici, Rice husk-derived carbon anodes for lithium ion batteries, J. Mater. Chem. 1 (2013) 5269–5273.
[31] J. Yang, Z. Ju, Y. Jiang, Z. Xing, B. Xi, J. Feng, S. Xiong, Enhanced capacity and rate capability of nitrogen/oxygen dual-doped hard carbon in capacitive potassium-ion storage, Adv. Mater. 30 (2018), 1700104.
[32] W. Cao, E. Zhang, J. Wang, Z. Liu, J. Ge, X. Yu, H. Yang, B. Lu, Potato derived biomass porous carbon as anode for potassium ion batteries, Electrochim. Acta 293 (2019) 364–370.
[33] Y. Chen, Z. Lu, L. Zhou, Y.-W. Mai, H. Huang, In situ formation of hollow graphitic carbon nanospheres in electrospun amorphous carbon nanofibers for high-performance Li-based batteries, Nanoscale 4 (2012) 6800–6805.
[34] N. Xiao, W.D. McCulloch, Y. Wu, Reversible dendrite-free potassium plating and stripping electrochemistry for potassium secondary batteries, J. Am. Chem. Soc. 139 (2017) 9475–9478.
[35] L. Wang, J. Zou, S. Chen, G. Zhou, J. Bai, P. Gao, Y. Wang, X. Yu, J. Li, Y.-S. Hu, TiS_2 as a high performance potassium ion battery cathode in ether-based electrolyte, Energy Storage Mater. 12 (2018) 216–222.
[36] Y. Li, Z. Yang, Z. Wu, J. Li, J. Zou, C. Jiang, J. Yang, L. Wang, X. Niu, The effects of lithium salt and solvent on lithium metal anode performance, Solid State Ionics 324 (2018) 144–149.
[37] L. Fan, S. Chen, R. Ma, J. Wang, L. Wang, Q. Zhang, E. Zhang, Z. Liu, B. Lu, Ultrastable potassium storage performance realized by highly effective solid electrolyte interphase layer, Small 14 (2018), 1801806.
[38] Z. Jian, W. Luo, X. Ji, Carbon electrodes for K-ion batteries, J. Am. Chem. Soc. 137 (2015) 11566–11569.
[39] F. Disma, L. Aymard, L. Dupont, J.M. Tarascon, Effect of mechanical grinding on the lithium intercalation process in graphites and soft carbons, J. Electrochem. Soc. 143 (1996) 3959–3972.
[40] L. Wang, J. Yang, J. Li, T. Chen, S. Chen, Z. Wu, J. Qiu, B. Wang, P. Gao, X. Niu, Graphite as a potassium ion battery anode in carbonate-based electrolyte and ether-based electrolyte, J. Power Sources 409 (2019) 24–30.
[41] T. Kogo, Y. Yoshida, K. Koganei, H. Matsumoto, T. Watanabe, J. Ogihara, T. Kasumi, Production of rice straw hydrolysis enzymes by the fungi trichoderma reesei and humicola insolens using rice straw as a carbon source, Bioresour. Technol. 233 (2017) 67–73.
[42] L. Xiao, Y. Cao, Delineating adsorption-insertion mechanism in hard carbon materials for sodium ion storage, in: ECS Meeting Abstracts, 2017, 486-486.
[43] D. Mitlin, High density sodium and lithium ion battery anodes from banana peels, in: ECS Meeting Abstracts, 2015, 477-477.